Inorganic Chemistry

Article

pubs.acs.org/IC

Hybrid Nanomaterials: Anchoring Magnetic Molecules on Naked Gold Nanocrystals

Rebecca J. Holmberg, Amy-Jayne Hutchings, Fatemah Habib, Ilia Korobkov, Juan C. Scaiano, and Muralee Murugesu*

Centre for Catalysis Research and Innovation and Department of Chemistry, University of Ottawa, Ottawa, Ontario, K1N 6N5, Canada

Supporting Information

ABSTRACT: The pairing of molecular magnets and nanomaterials couples top-down and bottom-up approaches to nanotechnology; facilitating a unique methodology to the controlled study of interfacial magnetic properties. Attaching Single-Molecule Magnets (SMMs) to "naked" gold nanoparticles is a novel method of exploring various avenues of magnetic nanotechnology, such as drug delivery, information storage, catalysis, and assembly of magnetic-nanostructural motifs. Herein we report the successful capping of laser ablation synthesized "naked" gold nanoparticles with a dinuclear dysprosium complex, while introducing new information regarding the changes in molecular magnetic properties upon surface attachment. We anticipate that this methodology in producing these magneto-plasmonic nanostructures not only provides answers to fundamental questions but also has the potential to provide new avenues to applications including information storage, multimodal imaging, biomedicine, and optoelectronics.

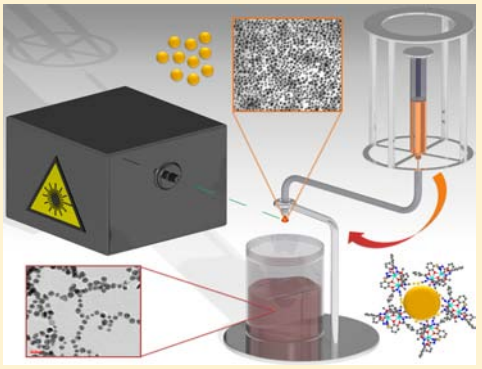

Merging bottom-up and top-down approaches in nanotechnology has the tremendous potential to open up an unexplored region in nanoscience. In recent years, several top-down synthetic approaches have been developed toward the isolation of various nanoparticles with unique properties.[1,2] Similarly, bottom-up approaches remain an important avenue for the fundamental study and application of small molecules.[3−5] However, combining these two systems in a controlled manner still remains an exciting challenge. If these two nanoatomic-scale materials are merged, we can envision harnessing their physical properties in order to create materials with multifunctional characteristics. With this in mind we have turned our attention toward anchoring molecular nanomagnets, termed Single-Molecule Magnets (SMMs), onto the surface of nanoparticles. In order to achieve this, we carefully chose a system where "naked" gold nanoparticles (AuNPs) provide an ideal surface for anchoring, without any obstruction from bulky surfactant molecules. An important advantage of AuNPs lies within their unique intrinsic optical and transport properties which have elicited their popularity in molecular marking, diagnostic imaging, and catalysis.[1,2,6−10] The selective affinity of gold to bind with sulfur (40−50 kcal mol^{-1} with a strength close to the Au−Au bond)[11,12] provides simple, customizable surface functionalization with sulfur-containing ligands. Thus, by functionalizing SMMs with such ligands, we can attach them to the surface of AuNPs, and form unique hybrid materials.

Single-molecule magnets represent a molecular approach to memory storage as they behave as single domain nanoscale magnetic entities with a barrier (U) to the reversal of the magnetization. This barrier arises from a combination of non-negligible ground state spin (S) and an appreciable uniaxial magnetic anisotropy (D).[13] In recent years, the quest for obtaining SMMs with high energy barriers led to the use of highly anisotropic lanthanide metal ions such as Dy^{III} and Tb^{III}.[14−20] Until recently, most SMMs were mainly studied in their pure molecular form; only a few examples show transition metal SMMs which have been successfully attached to a substrate,[21−23,28−33] and even fewer show this with lanthanide-based SMMs.[34−36] In order for SMMs to reach their potential as technologically viable materials, it is critical to maintain SMM behavior upon assembly into a functional device. The difficulty in such studies is in isolating a system which can offer an ideal surface for investigation using more practical techniques and traditional magnetometry as opposed to more rare and expensive techniques such as X-ray magnetic circular dichroism (XMCD). It is also a challenge to ascertain the magnetic properties once the SMM is attached to a bulk surface, as the bulk material will dilute the magnetic behavior of the molecular magnet. Due to these difficulties it is not well understood whether or not SMMs retain their slow magnetization relaxation properties after attachment. This is especially true knowing that recent studies demonstrate that lanthanide SMMs are susceptible to subtle changes in coordination environment and crystal field.[14,24−27] Few examples have been able to prove successful in retaining the magnetic

Received: October 26, 2013
Published: November 21, 2013

behavior of transition metal-based SMMs attached to a surface,[21−23,28,29] with merely one example for lanthanide based SMMs.[37] However, to our knowledge this has not yet been achieved using AuNPs as the substrate. A similar concept was illustrated for study of a paramagnetic radical complex which was grafted to a Au(111) single crystal surface through beam deposition.[38] Importantly, use of AuNPs has some distinct advantages, since the surface to volume ratio of the NPs in comparison to that of a bulk surface is high, allowing more SMMs per mass unit. Also, the suspension of particles can be studied using more readily available techniques, including traditional magnetometry, thus alleviating some of the challenges in studying surface attached SMM properties.

In parallel, spectacular developments have been made in NP synthesis, however, most synthesized nanoparticles have surfactants/ligands on their outer sphere to prevent agglomeration. Once isolated, ligand substitution becomes tedious over the entire surface of the NPs. Therefore, in order to anchor our SMMs to the surface of NP substrates we turned our attention toward a special class of NPs termed ligand-free NPs. These NPs are isolated through physical ablation of large polydisperse nanostructures in a liquid environment, and offer several advantages, such as efficient binding to desired molecules, a high molecule load without interference of secondary ligands, and low cleaning effort, as they do not interfere with the chemical residues. These monodispersed, size-tunable particles allow not only the amalgamation of bottom-up and top-down approaches, but also the combination of two or more properties in one material. Therefore, by combining magnetic properties of SMMs with optoelectronic properties of NPs, we target creation of hybrid materials with multifunctionalities.

Herein we report the successful capping of laser ablation synthesized water stable "naked" gold nanoparticles with a thiocyanate functionalized dinuclear dysprosium SMM ({Dy_2}), while retaining many of its unique magnetic properties. Simultaneously, we also introduce some unexpectedly different dynamic magnetic properties. We anticipate that this successful magnetic nanostructure will provide new fundamental information regarding the routes to future information storage applications of SMM-based nanomaterials. Also, through the inherent properties of this type of magnetic-plasmonic nanotechnology, new applications arise in optoelectronics, targeted imaging, separation, photothermal therapy, and many more potential applications.[39−43]

RESULTS AND DISCUSSION

The synthetic strategy for SMM capped AuNPs involved the design of a Dy-based complex functionalized with sulfur-exposed thiocyanate groups, thus, promoting its noncompetitive attachment to the surface of naked AuNPs. The chosen magnetic system, $[Dy^{III}_2(Hhmb)_3(NCS)_3]\cdot 2MeOH\cdot py$, {$Dy_2$}, (Figure 1) was based on previously successful application of *o*-vanillin derived lanthanide SMM complexes,[44−46] as well as the simplicity and high yield of Schiff base reactions. Specifically, the *N*′-(2-hydroxy-3-methoxybenzylidene)benzhydrazide (H_2hmb) ligand[45] was selected, as it produces multidentate coordinating pockets capable of accommodating two lanthanide metal centers. It also provides phenol oxygen atoms, which can be deprotonated to elicit a magnetic superexchange pathway through which the metal centers can interact. Dysprosium possesses unique magnetic properties such as magnetic anisotropy and a large spin ground state, while also having an

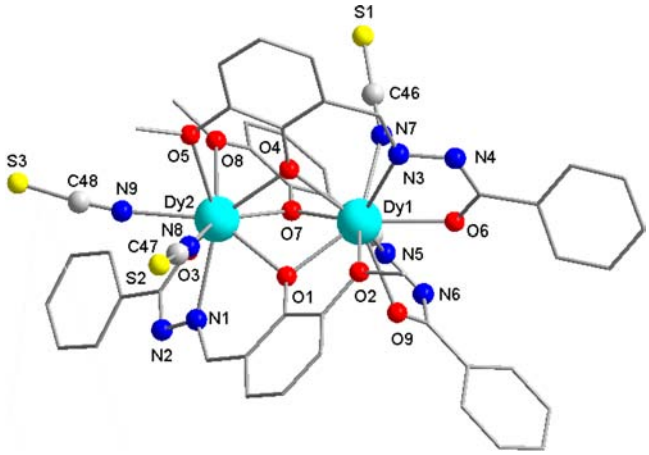

Figure 1. Partially labeled molecular structure of $[Dy^{III}_2(Hhmb)_3(NCS)_3]\cdot 2MeOH\cdot py$, ({$Dy_2$}), complex. Hydrogen atoms and solvent molecules have been removed for clarity.

inherently high coordination number in order to accommodate thiocyanate groups for binding to the gold surface. Through this methodology a dinuclear dysprosium complex (Figure 1) with three thiocyanate groups sterically available to bind to the surface of AuNPs was synthesized. The asymmetric complex is composed of a triple phenoxide bridged (O1, O4, and O7) dinuclear core encapsulated by three monoanionic $Hhmb^-$ ligands. The remaining coordination environment of the Dy centers is filled by one and two NCS^- molecules on Dy1 and Dy2, respectively. Both noncoordinated Dy(III) ions display a distorted monocapped square antiprism geometry with an intramolecular metal−metal distance of 3.56 Å and an average Dy−O−Dy angle of 99.3° (Tables S1−S2). The presence of MeOH in the crystal lattice provides an indication that the {Dy_2} complex is stable in MeOH as a solvent (*vide infra*).

The targeted synthesis of the AuNPs was derived from previous work,[1,2] in which the idea is to minimize the amount of potential surface agents present, thus, allowing custom derivatization of the particles themselves. Through utilizing hydrogen peroxide as a mild reducing agent, the byproducts become O_2 and H_2O, thus leaving behind a clean water-dispersed nanoparticle suspension. This is possible through irradiation of $AuCl_4^-$ in the presence of aqueous hydrogen peroxide, leading to a hydroperoxyl radical, $HOO^{\bullet}$, and its conjugate base, $O_2^{-\bullet}$, which operate as one-electron reducing agents.[1] Due to the potential for polydispersed agglomerated particle clusters, with only Cl^- on the particle periphery from the tetrachloroaurate precursor, the solution is then laser ablated in sequential drop form in order to create uniform particle shape, size, and distribution prior to the addition of a customized capping agent. In this work, the capping agent on AuNPs is the aforementioned {Dy_2}. This ultraclean synthetic method initially produces a solution of photochemically prepared gold nanostructures in water, which is placed into a syringe and slowly released into drops which are prealigned with a laser ablation setup (Figure S1). Once each drop has been ablated into uniform AuNPs, it is released into a solution of {Dy_2} in MeOH, where the Au−S bond can be formed, and particle nucleation and uncontrolled growth successfully halted.

Interestingly, during the procedure of centrifuging the colloidal suspensions it became apparent that the AuNPs were very challenging to isolate, as they would redistribute within solution once removed from the centrifuge. This

dx.doi.org/10.1021/ic4026975 | *Inorg. Chem.* 2013, 52, 14411−14418

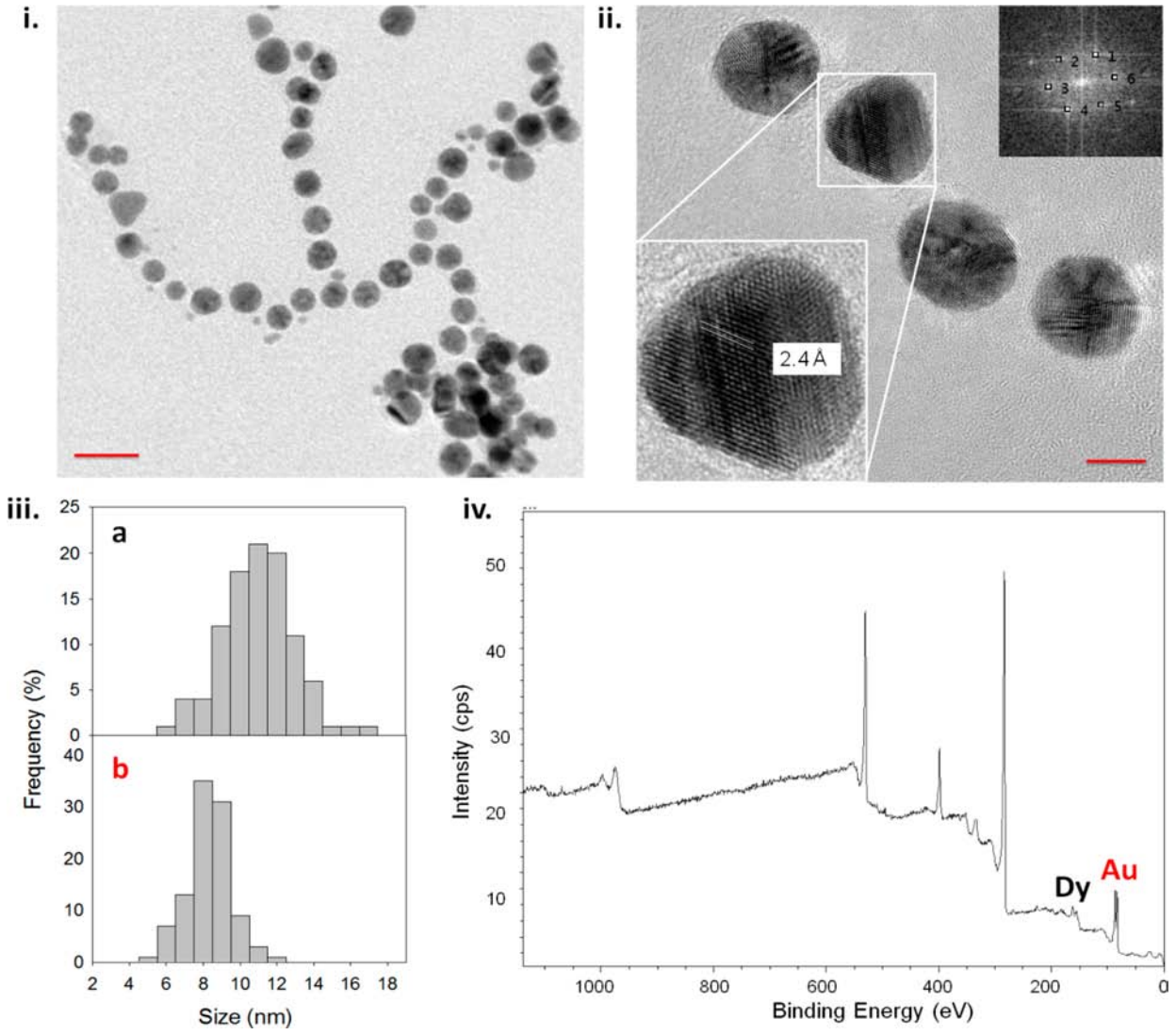

Figure 2. (i) TEM image of AuNPs capped with $\{Dy_2\}$. (ii) HRTEM image of AuNPs capped with $\{Dy_2\}$, displaying *d*-spacing of 2.4 Å and inset Fourier transform image. Scale bars: i. 20 nm, ii. 5 nm. (iii) Particle size distribution plots for AuNPs (a) and $\{Dy_2\}$-capped AuNPs (b). (iv) XPS spectrum of $\{Dy_2\}$-capped AuNPs, displaying the presence of Dy on the surface of the particles.

inevitably required high spinning speeds in order to force agglomeration. However, once capped with the $\{Dy_2\}$ they were easily precipitated with low spinning. This initial finding was consistent with our goal of capping the particles using this complex, and thus promoted further investigation. Isolated materials were investigated through a wide variety of techniques to confirm the composition, structure, as well as attachment of $\{Dy_2\}$ while maintaining its physical properties.

The first evidence of the successful attachment of the $\{Dy_2\}$ molecules onto the AuNP surface was provided by electron microscopy techniques. Scanning Electron Microscopy (SEM), Transmission Electron Microscopy (TEM), and High Resolution Transmission Electron Microscopy (HRTEM) images were taken in order to investigate the properties of uncapped gold nanoparticles versus those with surface bound SMMs. It is noteworthy to mention that the interaction between the capped particles caused the formation of chains to be observed. This phenomenon was then further explored in order to gain an understanding of what physical property is inducing the interaction, as well as how these networks are affecting the electronic and magnetic properties.

The parent naked AuNPs were initially studied using SEM in order to identify their size, shape, and distribution prior to coating the surface (Figure S2). From the images taken using SEM we were able to conclude that through the process of laser ablation the AuNPs became uniform in their rounded shape, and possessed a mean size of 11.0 nm. It was also clearly observed that the particles were distributed evenly across the grid, with no pattern of interaction between their surfaces. Similarly, the effects of a capping agent ($\{Dy_2\}$) on the particle size, shape, crystallinity, and distribution were studied using SEM, TEM, and HRTEM. TEM images of $\{Dy_2\}$-capped AuNPs clearly display a chain-like formation of particles (Figure 2.i.), which was not observed for uncapped AuNPs. These assemblies indicate an interaction between capping agents either magnetically or through peripheral ligand moieties. This interaction could promote magnetic translation of the particles, as well as chain-like formations. A control experiment was performed by adding an equal amount of MeOH, without $\{Dy_2\}$, to the AuNPs in order to confirm that the particle assembly was not inherent to the solvent, but the capping agent itself. It was confirmed through SEM imaging

dx.doi.org/10.1021/ic4026975 | *Inorg. Chem.* 2013, 52, 14411−14418

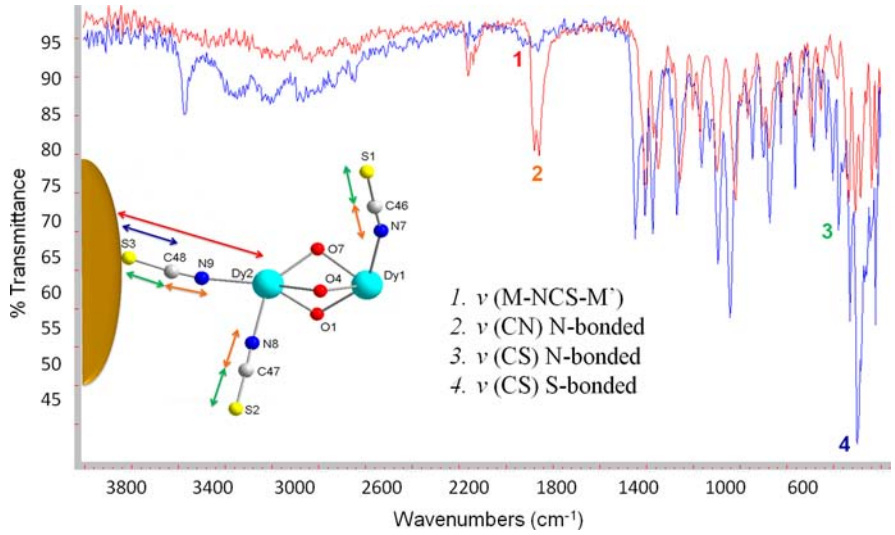

Figure 3. Infrared spectra comparing the $\{Dy_2\}$ (red), and AuNP capped with $\{Dy_2\}$ (blue), with specific SCN^- based stretches labeled and numbered.

that the particles were evenly distributed in MeOH. The AuNPs capped with $\{Dy_2\}$ display a crystalline *d*-spacing of 2.4 Å (Figure 2.ii.), indicative of Au (111) phase on the surface of the particles. The timing is crucial for SEM measurements as uncapped AuNPs continue to grow, thus, it was important to maintain a consistent time between laser ablation and drying the sample on a TEM grid. It is interesting to note that the average size of AuNP stopped at 8.3 nm (versus 11.0 nm) when capped with $\{Dy_2\}$ (Figure 2.iii.), and that there was a notable decrease in polydispersity of the capped AuNPs. This is primarily due to the capping agent arresting particle nucleation at a smaller diameter than if left uncapped, further confirming that the $\{Dy_2\}$ is indeed attached to the surface of the AuNPs.

Binding energy values are able to identify species on the surface of a material; thus, in order to further confirm the surface functionalization of AuNPs with the $\{Dy_2\}$, X-ray Photoelectron Spectroscopy (XPS) measurements were undertaken. These experiments clearly displayed a prominent Dy 4d peak on the surface with a binding energy of 155.0 eV (Figure 2.iv. and Table S3). This is a definitive confirmation of the presence of $\{Dy_2\}$ on the surface. The typical Au^0 4f doublet is also present, however, the binding energy is lower (82.5, 86.1 eV) compared to bulk Au values (~84, 87 eV); this is likely attributed to the surface modifications (attachment of $\{Dy_2\}$). We also observe the presence of an S 2p peak on the AuNP surface with a binding energy of 162.1 eV. These elements were then monitored as analytes using Inductively Coupled Plasma-Optical Emission Spectroscopy (ICP-OES), and can be found in Table S4. Measurements were performed on both solid and solution samples before and after the SMM capping agent was attached to AuNPs. The results indicate a ratio of 2:3 Dy:S, thus confirming the proposed structure both before and after adhesion. The presence of Dy after washing with $MeOH/H_2O$ and air drying the sample indicates the successful attachment of the desired $\{Dy_2\}$ capping agent to the AuNP surface.[47] Thus, we are able to observe distinct evidence of the presence of Dy on the AuNP surface through the use of a surface technique as well as one which measures the bulk sample.

To gain further insight into the Au−S linkage, as well as the retention of the structural features of the attached $\{Dy_2\}$ complex, Infrared (IR) analysis was carried out. Through comparative IR spectra, additional confirmation of the presence of a successful Au−S bond between the $\{Dy_2\}$ and AuNPs was obtained (Figure 3). Characteristic stretches for nitrogen bonded SCN^- groups were observed in the spectrum of $\{Dy_2\}$; specifically at ν(CN) = 2078(s), 2059(s) cm^{-1}, and ν(CS) = 858(s), 789(s) cm^{-1}.[48] The IR spectrum of AuNPs capped with $\{Dy_2\}$ also displayed characteristic nitrogen bonded SCN^- group stretches, as well as sulfur bonded stretches; specifically, a bridging M-NCS-M′ stretch was observed at ν(CN) = 2110(w) cm^{-1}, thus proving the connection through the thiocyanate group between Dy and Au. This was further confirmed by nitrogen bonded stretching observed at ν(CS) = 834(m), 805(m), and 779(m) cm^{-1}, and strong sulfur bonded stretching observed at ν(CS) = 700(s) cm^{-1}.[48] These characteristic stretches display the Au−S bond presence, as well as the confirmation of SCN^- bridging between the Dy metal center and AuNP, while retaining the stretches of the additional SCN^- groups bonded to Dy.

In order to confirm that the $\{Dy_2\}$ complex retained its structural integrity upon adhesion, characteristic stretches were investigated. The following vibration bands were observed within the spectra of $\{Dy_2\}$ and AuNP capped with $\{Dy_2\}$, respectively: ν(OH) = 3300 cm^{-1}, 3200 cm^{-1}; ν(NH) = 3170 cm^{-1}, 3165 cm^{-1}; ν(CH, Ar−H) = 3065 cm^{-1}, 3062 cm^{-1}; ν(CH, O−CH_3) = 2943 cm^{-1}, 2940 cm^{-1}; ν(C═N) = 1605 cm^{-1}, 1605 cm^{-1}; ν(CO, Ar−O) = 1296 cm^{-1}, 1299 cm^{-1}. Further confirmation was obtained by vibration bands displaying the metal coordination, through oxygen, to a ligand phenyl group: $\nu(M-O-Ar)_{\{Dy2\}}$ = 1243 cm^{-1}, 1147 cm^{-1} and $\nu(M-O-Ar)_{\{AuNP-Dy2\}}$ = 1235 cm^{-1} and 1150 cm^{-1}.[49]

To clearly demonstrate the stability of our $\{Dy_2\}$ in employed solvents, IR spectra and Powder X-ray Diffraction (PXRD) were also taken of the $\{Dy_2\}$ after its dissolution in MeOH and water (the composition of the colloidal AuNP solution). The obtained IR spectrum is superimposable on that of crystalline $\{Dy_2\}$ (Figure 3, in red), thus confirming retention of its structural integrity (Figure S3). PXRD experiments showed that the powder obtained after dissolution and drying, compared with the pattern from single crystal XRD experiments, exhibited definite matching of peaks (Figure

dx.doi.org/10.1021/ic4026975 | *Inorg. Chem.* 2013, 52, 14411−14418

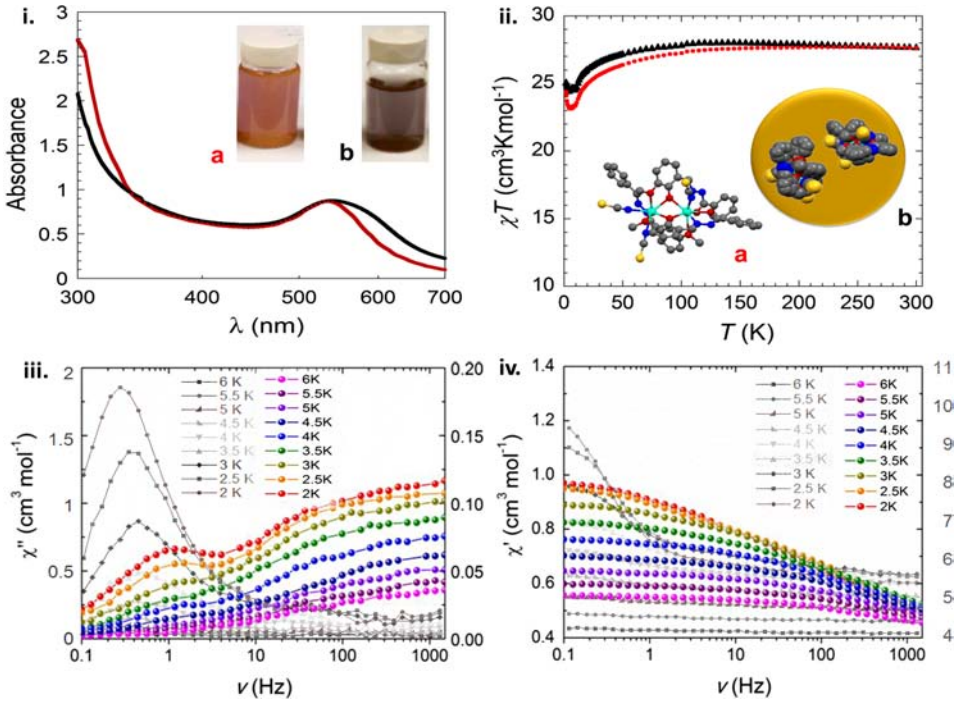

Figure 4. (i) UV−vis spectra of uncapped AuNPs, solution color shown in (a), and AuNPs capped with $\{Dy_2\}$, solution color shown in (b). (ii) Temperature dependence of the χT product at 1000 Oe for $\{Dy_2\}$ (a), and for AuNPs capped with $\{Dy_2\}$ (b). (iii) Frequency dependence of the out-of-phase susceptibility (χ'') and (iv) the in-phase (χ') ac susceptibility for the $\{Dy_2\}$ (gray scale), and AuNPs capped with $\{Dy_2\}$ (colored), from 2 to 6 K under applied 1000 and 3000 Oe static fields, respectively.

S4.ii.a. and b.), and thus the structural integrity is successfully maintained.

PXRD patterns were also employed for comparison between the patterns of uncapped and capped AuNPs. These experiments were initially performed on AuNPs (Figure S4.i.a.), followed by AuNPs capped with $\{Dy_2\}$ (Figure S4.i.b.). The pattern for AuNPs displayed a prominent (111) peak (JCPDS 001−1172), which corresponds to the *d*-spacing value of 2.4 Å found by taking the Fourier transform of HRTEM images (Figure 2.ii.). This is not surprising as (111) is a common crystalline phase for gold materials, and importantly is often the phase employed in sulfur−gold surface bonding studies.[50] This reveals a well ordered nanoparticle, which can accommodate ordering of sulfur bonds across its surface. There were also peaks from (200), (220), and (311) lattice planes, which were expected to be found within the chosen 2θ range for AuNPs. This pattern was then compared with that of the $\{Dy_2\}$-capped AuNP. The peaks present in the AuNP pattern were also present in the pattern of $\{Dy_2\}$-capped AuNP, indicating that the AuNPs retained their crystalline surface structure. However, it should also be noted that peak intensity was lower and broader in full width at half-maximum, thus confirming the smaller size distribution of the particles capped with $\{Dy_2\}$.

It is important that we not ignore the plasmonic properties of AuNPs, and their ability to be utilized as a method for detection of surface modification. The attachment of the $\{Dy_2\}$ to the AuNP surface had a distinct effect on the UV−vis spectroscopic properties of the AuNPs, shifting and broadening the characteristic plasmon band at 530 nm (Figure 4.i.).[51] This effect confirms the alteration of the surface plasmonic properties through an attached moiety. We can also observe the distinct change in coloration between the laser ablated AuNPs (Figure 4.i.a) and those capped with $\{Dy_2\}$ (Figure 4.i.b), indicative of the change in plasmonic properties through surface alteration of the particles. Thus, this confirms the presence of the $\{Dy_2\}$ molecules on the surface of the AuNPs. Also, the increased scattering at lower energy is indicative of the capped particle association seen by electron microscopy forming directly in the colloidal solution. The chain-like networks of capped nanoparticles are, therefore, forming rapidly in solution, which has previously been observed through the use of a connector ligand between particles.[52] UV−vis measurements were also utilized in calculating a total gold concentration (based on absorbance 0.9) of 0.28 mM,[51] corresponding to [AuNP] of 16.0 nM based on 8.3 nm diameter particles, having about 17 750 atoms per particle, of which 3322 are on the surface (Table S5). This concentration value is very close to the initial Au concentration of 0.33 mM. Taking into account the parameters in Table S5, as well as the longest measured distance across the $\{Dy_2\}$ molecule with a potential S−Au binding site of 18.53 Å between H13A-H28A, we can estimate the number of SMMs attached to the surface of one AuNP (∼20 molecules).

Finally, in order to probe the magnetic behavior of the $\{Dy_2\}$, as well as the $\{Dy_2\}$-capped AuNPs, direct and alternating current (dc and ac) susceptibility measurements were performed using a Superconducting Quantum Interference Device (SQUID) magnetometer. Variable temperature dc and ac susceptibility measurements were performed on polycrystalline $\{Dy_2\}$ and powder $\{Dy_2\}$-capped AuNPs. Similar behavior was observed for the dc measurements (Figure 4.ii). At room temperature the observed χT value for the $\{Dy_2\}$ of 27.65 cm^3 K mol^{-1} is slightly lower than the theoretical value of 28.34 cm^3 K mol^{-1} for two noninteracting Dy^{III} ions ($^6H_{15/2}$, $S = 5/2$, $L = 5$, $g = 4/3$, $\chi T = 14.17$ cm^3 K mol^{-1}). The room temperature χT value for the $\{Dy_2\}$-capped AuNPs is very close to that of the $\{Dy_2\}$. The χT product remains stable upon decrease in temperature, until 175 K where the $\{Dy_2\}$ displays a

dx.doi.org/10.1021/ic4026975 | *Inorg. Chem.* 2013, 52, 14411−14418

gradual decrease before a more dramatic drop to 21.14 cm^3 K mol^{-1} at 5.4 K, the behavior of which is mimicked by $\{Dy_2\}$-capped AuNPs which drop at 4.5 K. This decrease can be attributed to the presence of significant anisotropy for Dy^{III} ions. Below 4.5 K the observed rapid increase of the χT product indicates the presence of non-negligible ferromagnetic interaction between Dy^{III} ions at low temperature. The smallest intermolecular Dy···Dy distance being 8.56 Å, with the intramolecular Dy···Dy distance being 3.56 Å, indicates the observed ferromagnetic interaction most likely arises from the intramolecular interactions. This is further confirmed by the fact the attached $\{Dy_2\}$-molecules also exhibit similar behavior in which the intermolecular distances are now increased upon attachment.

Slow magnetic relaxation dynamic studies were performed using ac susceptibility measurements at various temperatures and applied dc fields. Under zero-applied static field, no ac signal was observed for both samples; however, upon application of a static dc field the appearance of the ac signal is indicative of field-induced SMM-like behavior. Such behavior is indicative of significant quantum tunnelling of the magnetization (QTM) occurring under zero applied field. To optimize the slow relaxation process through the reduction of QTM, optimal field measurements, where the minimum of the characteristic frequency is observed, were carried out. The optimum fields were found to be 1000 Oe for $\{Dy_2\}$ and 3000 Oe for $\{Dy_2\}$-capped AuNPs. Selected frequency (ν) dependent in-phase (χ') and out-of-phase magnetic susceptibility (χ'') plots for both systems at the indicated temperatures are shown in Figure 4.iii. and iv. It is noteworthy that even with the applied static field a minimal shift was observed in the peak maxima indicative of the presence of significant QTM. This was further confirmed by obtaining the effective energy barrier and relaxation time through the fit using the Arrhenius equation ($\tau = \tau_0 \exp(U_{eff}/kT)$, which resulted in a value of U_{eff} = 2.4 K (τ_0 = 0.16 s). When attached to AuNPs, the $\{Dy_2\}$ experiences significant change in ac signal dynamics and an increase in QTM, thus not allowing for the accurate determination of an energy barrier. This change can be attributed to change in local anisotropy of the Dy ions upon binding of $\{Dy_2\}$ molecules to the AuNP surface through the SCN^- moiety.[53,54] This important discovery clearly indicates that upon attachment dc magnetic properties are retained while there is a change in dynamic behavior. Such an effect of the second coordination environment on relaxation dynamics has recently been reported in molecular systems,[55,56] however, to our knowledge never before witnessed in a hybrid nanomaterial. This result cautions us about application potential of SMMs on surfaces for the creation of new molecular electronic devices.

CONCLUSION

Throughout the study, it has constantly become apparent that we are able not only to synthetically produce a unique SMM structure and produce remarkable naked gold nanoparticles, but also to combine the two entities into one hybrid superstructure. A dysprosium-based SMM structure was produced and studied, followed by its proven successful attachment to uniquely fabricated naked gold nanoparticles. Once attached, the material was studied extensively and found to retain the dc magnetic properties of the SMM, while exhibiting a change in the dynamic magnetic properties. Thus, these findings introduce a new variable to the field of molecular magnetism, which is not merely the ability of a magnet to retain the magnetic properties on a surface, but instead the ability to change those properties to suit the desired application through attachment. The ability to study the properties of SMMs on surfaces has the potential to become a much more comprehensive process utilizing more varied techniques than before. In the future, the plasmonic properties and their potential effects on magnetic behavior of SMMs will be a fascinating exploration, as well as the fragile optimization of the properties of binding mode and capping agent. This successful coupling of top-down and bottom-up chemistry is a truly unique methodology and opens up the field of molecular magnetism to a new realm of application possibilities.

METHODS

All manipulations were performed under aerobic/ambient conditions. All reagents were purchased from the following sources: Alfa Aesar, Acros Organics, Strem Chemicals, TCI, and Sigma Aldrich. All reagents were employed without further purification.

$[Dy^{III}_2(Hhmb)_3(NCS)_3]\cdot 2MeOH\cdot py$ ($\{Dy_2\}$). This was synthesized by initially dissolving $DyCl_3\cdot 6H_2O$ (0.25 mmol, 0.094 g) in 5 mL MeOH, which was then added to a solution of H_2hmb (0.25 mmol, 0.067 g), NaSCN (1.0 mmol, 0.081 g) in 5 mL MeOH, and pyridine (1.0 mmol, 0.078 mL). Synthetic procedure for H_2hmb ligand can be found in the Supporting Information. The yellow-colored solution was stirred for 5 min, filtered, and placed in an ether bath at room temperature. X-ray quality yellow block crystals were recovered after 3 days. Crystals were collected by vacuum filtration. Yield: 32%.

Au Nanoparticles (AuNP). These were synthesized using a slightly modified photochemical procedure which was employed previously using hydrogen peroxide as a reducing agent.[1,2] An aqueous solution of 35 wt.% H_2O_2 and 0.33 mM $NaAuCl_4$ in Millipore water was irradiated in a well plate for 10 min using 14 UVA lamps in a LZC-L4 V photoreactor (Luzchem Research, Inc.). The AuNPs were initially characterized using UV−visible spectroscopy, revealing the presence of a broad plasmon band centered at 530 nm, and extensive light scattering at 800 nm. ICP-OES measurements allowed the calculation of the number of Au atoms per particle, 17 750 (Table S5).

Laser Drop Ablation. This was performed with frequency-doubled 532 nm (8 ns) pulses from a Continuum Q-switched Nd:YAG laser. The beam was focused on the drop of reduced Au solution, which was generated by a computer-controlled syringe pump mechanism. This mechanism was automated to create equal drop formations (volume 7−10 μL) through a Teflon tube (1.6 mm diameter). Photographs and videos were taken with a Nikon D90 DSLR camera equipped with a Sigma 105 mm f 2.8 macrolens, controlled by the same software as the laser-drop system. Irradiated drops were collected in a cuvette containing the desired capping agent/stabilizer. A schematic diagram of the laser drop system is shown in Figure S1.

Infrared Spectrometry. IR spectra were recorded on all samples in the solid state on a Varian 640 FT-IR spectrometer in the 575−4000 cm^{-1} range.

ICP-OES. Inductively coupled plasma optical emission spectrometry measurements were performed using a Varian Vista Pro CCD-ICP-OES Spectrometer. Each sample was digested separately, in triplicate, prior to analysis. The triplicates agreed well, and were averaged to obtain the final analyte relationship calculations. Each element was monitored at more than one wavelength in order to validate the data and rule out interferences. All concentrations were calculated in ppm (w/w basis), and are presented as percentage composition values.

Single Crystal X-ray and Powder X-ray Crystallography. Single crystal X-ray diffraction experiments were performed on $[Dy^{III}_2(Hhmb)_3(NCS)_3]\cdot 2MeOH\cdot py$. A Bruker APEX-II CCD device was used to collect the unit cell and intensity data using graphite Mo−Kα radiation (λ = 0.71073 Å). Data reduction included correction for Lorentz and polarization effects, with an applied multiscan absorption correction (SADABS). Crystal structures were solved and refined using the SHELXTL program suite. Direct methods yielded all non-

dx.doi.org/10.1021/ic4026975 | Inorg. Chem. 2013, 52, 14411−14418

hydrogen atoms which were refined with anisotropic thermal parameters. All hydrogen atom positions were calculated geometrically and were riding on their respective atoms.

X-ray powder diffraction experiments were performed using a RIGAKU Ultima IV, equipped with a Cu−Kα radiation source (λ = 1.541 836 Å), and a graphite monochromator. Scanning of the 2θ range was performed from 5° to 40°, depending on the particular sample. In order to assign the peaks corresponding to particular crystalline phases, PDXL software equipped with the RIGAKU apparatus was used with the ICDD database.

SEM/TEM. Scanning electron microscopy images were taken to elicit the size and shape of the particles using a JSM-7500F FESEM (JEOL), and transmission electron images were taken to obtain better resolution images of particles with a JEM-2100F FETEM (JEOL). HR-TEM (JEOL JEM-2100F) was used to study the intrinsic crystallography of the samples.

XPS. Surface analysis by XPS was performed using a Kratos Axis Ultra DLD spectrometer employing a monochromated Al Kα X-ray source at 140 W of X-ray energy.

SQUID. Magnetic measurements were performed using a Quantum Design SQUID magnetometer MPMS-XL7, operating between 1.8 and 300 K for dc-applied fields ranging from −7 to 7 T. Susceptibility measurements were performed on both sample types: freshly filtered crushed polycrystalline sample of 9.1 mg {Dy_2} in grease, and powder sample of 32.7 mg {Dy_2}-capped AuNPs, wrapped within polyethylene membranes. Direct current (dc) susceptibility measurements were performed at 1000 Oe, and alternating current (ac) susceptibility measurements were performed under an oscillating ac field of 3 Oe and applied dc field of 1000 Oe for the {Dy_2} and 3000 Oe for the {Dy_2}-capped AuNPs with ac frequencies ranging from 0.1 to 1500 Hz. The magnetization data was initially collected at 100 K to check for ferromagnetic impurities, found to be absent in all samples.

■ ASSOCIATED CONTENT

Ⓢ Supporting Information

Details of crystallographic information of {Dy_2}, experimental details, IR, SQUID magnetic measurements, and supplementary figures. This material is available free of charge via the Internet at http://pubs.acs.org.

■ AUTHOR INFORMATION

Corresponding Author

*E-mail: m.murugesu@uottawa.ca.

Author Contributions

The manuscript was written through contributions of all authors. All authors have given approval to the final version of the manuscript. R.J.H. synthesized AuNPs, designed and performed experiments, analyzed data, and wrote the manuscript; A-J.H. synthesized the {Dy_2} complex; F.H. performed magnetic measurements on {Dy_2}; I.K. performed single crystal XRD on {Dy_2}; M.M. and J.C.S. supervised this work and aided in manuscript writing/editing.

Notes

The authors declare no competing financial interest.

■ ACKNOWLEDGMENTS

We gratefully acknowledge financial support towards this project from the NSERC of Canada. Special thanks to Dr. Kevin Stamplecoskie and Mr. Michel Grenier for technical help and support.

■ REFERENCES

(1) McGilvray, K. L.; Granger, J.; Correia, M.; Banks, J. T.; Scaiano, J. C. *Phys. Chem. Chem. Phys.* **2011**, *13*, 11914−11918.

(2) Bueno-Alejo, C. J.; D'Alfonso, C.; Pacioni, N. L.; González-Béjar, M.; Grenier, M.; Lanzalunga, O.; Alarcon, E. I.; Scaiano, J. C. *Langmuir* **2012**, *28*, 8183−8189.

(3) Sessoli, R.; Powell, A. K. *Coord. Chem. Rev.* **2009**, *253*, 2328−2341.

(4) Yan, P.-F.; Lin, P.-H.; Habib, F.; Aharen, T.; Murugesu, M.; Deng, Z.-P.; Li, G.-M.; Sun, W.-B. *Inorg. Chem.* **2011**, *50*, 7059−7065.

(5) Bellido, E.; Cardonna-Serra, S.; Coronado, E.; Ruiz-Molina, D. *Chem. Commun.* **2011**, *47*, 5175−5177.

(6) Ben-Yakar, A.; Eversole, D.; Ekici, O. Spherical and Anisotropic Gold Nanomaterials in Plasmonic Laser Phototherapy of Cancer. In *Non-Magnetic Metallic Nanomaterials for Life Sciences*; Kumar, C., Ed.; John Wiley & Sons: New York, 2008; pp 493−539.

(7) Jain, P. K.; Huang, X.; El-Sayed, I. H.; El-Sayed, M. A. *Acc. Chem. Res.* **2008**, *41*, 1578−1586.

(8) Grisel, R.; Weststrate, K.-J.; Gluhoi, A.; Nieuwenhuys, B. E. *Gold Bull.* **2002**, *35*, 39−45.

(9) Corma, A.; Garcia, H. *Chem. Soc. Rev.* **2008**, *37*, 2096−2126.

(10) Ahn, W.; Hong, Y.; Boriskina, S. V.; Reinhard, B. M. *ACS Nano* **2013**, *7*, 4470−4478.

(11) Hakkinen, H. *Nat. Chem.* **2012**, *4*, 443−455.

(12) Pensa, E.; Cortes, E.; Corthey, E.; Carro, G.; Vericat, C.; Fonticelli, M. H.; Benitez, G.; Rubert, A. A.; Salvarezza, R. C. *Acc. Chem. Res.* **2012**, *45*, 1183−1192.

(13) Jurca, T.; Farghal, A.; Lin, P.-H.; Korobkov, I.; Murugesu, M.; Richeson, D. S. *J. Am. Chem. Soc.* **2011**, *133*, 15814−15817.

(14) Habib, F.; Murugesu, M. *Chem. Soc. Rev.* **2013**, *42*, 3278−3288.

(15) Chibotaru, L. F.; Ungur, L.; Soncini, A. *Angew. Chem., Int. Ed.* **2008**, *47*, 4126−4129.

(16) Hussain, B.; Savard, D.; Burchell, T. J.; Wernsdorfer, W.; Murugesu, M. *Chem. Commun.* **2009**, 1100−1102.

(17) Gamer, M. T.; Lan, Y. H.; Roesky, P. W.; Powell, A. K.; Clerac, R. *Inorg. Chem.* **2008**, *47*, 6581−6583.

(18) Bernot, K.; Luzon, J.; Bogani, L.; Etienne, M.; Sangregorio, C.; Shanmugam, M.; Caneschi, A.; Sessoli, R.; Gatteschi, D. *J. Am. Chem. Soc.* **2009**, *131*, 5573−5579.

(19) Bernot, K.; Pointillart, F.; Rosa, P.; Etienne, M.; Sessoli, R.; Gatteschi, D. *Chem. Commun.* **2010**, *46*, 6458−6460.

(20) Bi, Y. F.; Wang, X. T.; Liao, W. P.; Wang, X. W.; Deng, R. P.; Zhang, H. J.; Gao, S. *Inorg. Chem.* **2009**, *48*, 11743−11747.

(21) Mannini, M.; Pineider, F.; Sainctavit, P.; Danieli, C.; Otero, E.; Sciancalepore, C.; Talarico, A. M.; Arrio, M.-A.; Cornia, A.; Gatteschi, D.; Sessoli, R. *Nat. Mater.* **2009**, *8*, 194−197.

(22) Gomez-Segura, J.; Veciana, J.; Ruiz-Molina, D. *Chem. Commun.* **2007**, *36*, 3699−3707.

(23) Moro, F.; Corradini, V.; Evangelisti, M.; De Renzi, V.; Biagi, R.; del Pennino, U.; Milios, C. J.; Jones, L. F.; Brechin, E. K. *J. Phys. Chem. B* **2008**, *112*, 9729−9735.

(24) Lin, P.-H.; Sun, W.-B.; Yu, M.-F.; Li, G.-M.; Yan, P.-F.; Murugesu, M. *Chem. Commun.* **2011**, *47*, 10993−10995.

(25) Cucinotta, G.; Perfetti, M.; Luzon, J.; Etienne, M.; Car, P.-E.; Caneschi, A.; Calvez, G.; Bernot, K.; Sessoli, R. *Angew. Chem., Int. Ed.* **2012**, *51*, 1606−1610.

(26) Sakaue, S.; Fuyuhiro, A.; Fukuda, T.; Ishikawa, N. *Chem. Commun.* **2012**, *48*, 5337−5339.

(27) Rajeshkumar, T.; Rajaraman, G. *Chem. Commun.* **2012**, *48*, 7856−7858.

(28) Zobbi, L.; Mannini, M.; Pacchioni, M.; Chastanet, G.; Bonacchi, D.; Zanardi, C.; Biagi, R.; Del Pennino, U.; Gatteschi, D.; Cornia, A.; Sessoli, R. *Chem. Commun.* **2005**, *12*, 1640−1642.

(29) Mannini, M.; Pineider, F.; Danieli, C.; Totti, F.; Sorace, L.; Sainctavit, P.; Arrio, M. -A.; Otero, E.; Joly, L.; Cezar, J. C.; Cornia, A.; Sessoli, R. *Nature* **2010**, *468*, 417−422.

(30) Saywell, A.; Magnano, G.; Satterley, C. J.; Perdigao, L. M. A.; Britton, A. J.; Taleb, N.; Gimenez-Lopez, M. d. C.; Champness, N. R.; O-Shea, J. N.; Beton, P. H. *Nat. Commun.* **2010**, *1*, 75.

(31) Naitabdi, A.; Bucher, J.-P.; Gerbier, P.; Rabu, P.; Drillon, M. *Adv. Mater.* **2005**, *17*, 1612−1616.

(32) Petraki, F.; Peisert, H.; Aygul, U.; Latteyer, F.; Uihlein, J.; Vollmer, A.; Chasse, T. *J. Phys. Chem. C* **2012**, *116*, 11110−11116.
(33) Domingo, N.; Bellido, E.; Ruiz-Molina, D. *Chem. Soc. Rev.* **2012**, *41*, 258−302.
(34) Vitali, L.; Fabris, S.; Conte, A. M.; Brink, S.; Ruben, M.; Baroni, S.; Kern, K. *Nano Lett.* **2008**, *8*, 3364−3368.
(35) Gonidec, M.; Biagi, R.; Corradini, V.; Moro, F.; De Renzi, V.; del Pennino, U.; Summa, D.; Muccioli, L.; Zannoni, C.; Amabilino, D. B.; Veciana, J. *J. Am. Chem. Soc.* **2011**, *133*, 6603−6612.
(36) Stepanow, S.; Honolka, J.; Gambardella, P.; Vitali, L.; Abdurakhmanova, N.; Tseng, T.-C.; Rauschenbach, S.; Tait, S. L.; Sessi, V.; Klyatskaya, S.; Ruben, M.; Kern, K. *J. Am. Chem. Soc.* **2010**, *132*, 11900−11901.
(37) Vincent, R.; Klyatskaya, S.; Ruben, M.; Wernsdorfer, W.; Balestro, F. *Nature* **2012**, *488*, 357−360.
(38) Savu, S. −A.; Biswas, I.; Sorace, L.; Mannini, M.; Rovai, D.; Caneschi, A.; Chasse, T.; Casu, M. B. *Chem.—Eur. J.* **2013**, *19*, 3445−3450.
(39) Fan, Z.; Shelton, M.; Singh, A. K.; Senapati, D.; Khan, S. A.; Ray, P. C. *ACS Nano* **2012**, *6*, 1065−1073.
(40) Gao, J.; Gu, H.; Xu, B. *Acc. Chem. Res.* **2009**, *42*, 1097−1107.
(41) Levin, C. S.; Hofmann, C.; Ali, T. A.; Kelly, A. T.; Morosan, E.; Nordlander, P.; Whitmire, K. H.; Halas, N. J. *ACS Nano* **2009**, *3*, 1379−1388.
(42) Sotiriou, G. A.; Hirt, A. M.; Lozach, P.-Y.; Teleki, A.; Krumeich, F.; Pratsinis, S. E. *Chem. Mater.* **2011**, *23*, 1985−1992.
(43) Lee, S.-M.; Kim, H. J.; Ha, Y.-J.; Park, Y. N.; Lee, S.-K.; Yoo, K.-H. *ACS Nano* **2013**, *7*, 50−57.
(44) Costes, J.-P.; Dahan, F.; Nicodème, F. *Inorg. Chem.* **2001**, *40*, 5285−5287.
(45) Lin, P.-H.; Burchell, T. J.; Ungur, L.; Chibotaru, L. F.; Wernsdorfer, W.; Murugesu, M. *Angew. Chem.* **2009**, *48*, 9489−9492.
(46) Lin, P.-H.; Korobkov, I.; Burchell, T. J.; Murugesu, M. *Dalton Trans.* **2012**, *41*, 13649−13656.
(47) Hinterwirth, H.; Kappel, S.; Waitz, T.; Prohaska, T.; Lindner, W.; Lammerhofer, M. *ACS Nano* **2013**, *7*, 1129−1136.
(48) Nakamoto, K. *Infrared and Raman Spectra of Inorganic and Coordination Compounds*, 3rd ed.; Wiley Interscience, 1978.
(49) Ozay, H.; Yildiz, M.; Kiraz, A. *Crystallogr. Rep.* **2013**, *58*, 106−110.
(50) Häkkinen, H. *Nat. Chem.* **2012**, *4*, 443−455.
(51) Scaiano, J. C.; Stamplecoskie, K. *J. Phys. Chem. Lett.* **2013**, *4*, 1177−1187.
(52) DeVries, G. A.; Brunnbauer, M.; Hu, Y.; Jackson, A. M.; Long, B.; Neltner, B. T.; Uzun, O.; Wunsch, B. H.; Stellacci, F. *Science* **2007**, *315*, 358−361.
(53) Moro, F.; Corradini, V.; Evangelisti, M.; Biagi, R.; De Renzi, V.; del Pennino, U.; Cezar, J. C.; Inglis, R.; Milios, C. J.; Brechin, E. K. *Nanoscale* **2010**, *2*, 2698−2703.
(54) Otero, G.; Evangelio, E.; Rogero, C.; Vazquez, L.; Gomez-Segura, J.; Gago, J. J.; Ruiz-Molina, D. *Langmuir* **2009**, *25*, 10107−10115.
(55) Boulon, M.-E.; Cucinotta, G.; Luzon, J.; Degl'Innocenti, C.; Perfetti, M.; Bernot, K.; Calvez, G.; Caneschi, A.; Sessoli, R. *Angew. Chem., Int. Ed.* **2013**, *52*, 350−354.
(56) Le Roy, J. J.; Jeletic, M.; Gorelsky, S. I.; Korobkov, I.; Ungur, L.; Chibotaru, L. F.; Murugesu, M. *J. Am. Chem. Soc.* **2013**, *135*, 3502−3510.